PNAS RESEARCH ARTICLE | GENETICS

Identification of *PSMB5* as a genetic modifier of fragile X–associated tremor/ataxia syndrome

Ha Eun Kong[a], Junghwa Lim[a], Alexander Linsalata[b], Yunhee Kang[a], Indranil Malik[b], Emily G. Allen[a], Yiqu Cao[a], Lisa Shubeck[a], Rich Johnston[a], Yanting Huang[c], Yanghong Gu[d], Xiangxue Guo[a], Michael E. Zwick[a], Zhaohui Qin[c], Thomas S. Wingo[a,e], Jorge Juncos[e], David L. Nelson[d], Michael P. Epstein[a], David J. Cutler[a], Peter K. Todd[b], Stephanie L. Sherman[a], Stephen T. Warren[a,f,g,1], and Peng Jin[a,2]

Edited by Hugo Bellen, Baylor College of Medicine, Houston, TX; received October 5, 2021; accepted March 17, 2022

Fragile X–associated tremor/ataxia syndrome (FXTAS) is a debilitating late-onset neurodegenerative disease in premutation carriers of the expanded CGG repeat in *FMR1* that presents with a spectrum of neurological manifestations, such as gait ataxia, intention tremor, and parkinsonism [P. J. Hagerman, R. J. Hagerman, *Ann. N. Y. Acad. Sci.* 1338, 58–70 (2015); S. Jacquemont *et al.*, *JAMA* 291, 460–469 (2004)]. Here, we performed whole-genome sequencing (WGS) on male premutation carriers ($CGG_{55–200}$) and prioritized candidate variants to screen for candidate genetic modifiers using a *Drosophila* model of FXTAS. We found 18 genes that genetically modulate CGG-associated neurotoxicity in *Drosophila*, such as *Prosbeta5* (*PSMB5*), *pAbp* (*PABPC1L*), *e(y)1* (*TAF9*), and *CG14231* (*OSGEPL1*). Among them, knockdown of *Prosbeta5* (*PSMB5*) suppressed CGG-associated neurodegeneration in the fly as well as in N2A cells. Interestingly, an expression quantitative trait locus variant in *PSMB5*, $PSMB5^{rs11543947\text{-}A}$, was found to be associated with decreased expression of *PSMB5* and delayed onset of FXTAS in human *FMR1* premutation carriers. Finally, we demonstrate evidence that *PSMB5* knockdown results in suppression of CGG neurotoxicity via both the RAN translation and RNA-mediated toxicity mechanisms, thereby presenting a therapeutic strategy for FXTAS.

FMR1 | FXTAS | premutation | fragile X syndrome | PSMB5

Significance

Expansion of 55-200 CGG repeats in the 5′ untranslated region of *FMR1* predisposes carriers to fragile X–associated tremor/ataxia syndrome (FXTAS), a late-onset neurodegenerative disorder. FXTAS demonstrates incomplete penetrance, which strongly suggests the presence of genetic modifiers. We performed whole-genome sequencing (WGS) on male premutation carriers ($CGG_{55–200}$) followed by a functional screen in *Drosophila* and identified *PSMB5* as a strong suppressor of CGG-associated neurodegeneration, thereby presenting a therapeutic strategy for FXTAS.

Fragile X–associated tremor/ataxia syndrome (FXTAS) is a late-onset neurodegenerative debilitating disorder characterized by cerebellar dysfunction, with the main clinical presentations of intention tremor and cerebellar ataxia (1, 2). Premutation carriers with 55 to 200 expanded unmethylated CGG repeats in the 5′ untranslated region (UTR) of *FMR1* are predisposed to developing FXTAS. On average, individuals in the general population carry 30 CGG repeats, whereas CGG repeats greater than 200 lead to fragile X syndrome (FXS) due to DNA methylation-mediated silencing of *FMR1* transcription and translation (3–6). Importantly, premutation carriers are not rare in the population, with an estimated prevalence of about 1:250 women and 1:800 men (7–9). A persisting conundrum is that not all premutation carriers develop FXTAS; ∼40% of males and 16% of females develop FXTAS in late adulthood (1, 2). The incomplete penetrance of FXTAS has motivated the search for genetic modifiers that may serve as genetic biomarkers for prognosis and potential therapeutic targets (10).

Our current understanding of the pathogenesis of FXTAS stands by two main proposed mechanisms: RNA toxicity and repeat-associated non-AUG (RAN) translation. The RNA toxicity mechanism of FXTAS pathogenesis results from sequestration of key RNA binding proteins to the expanded CGG repeats, preventing them from performing their normal physiological function (10). The RNA-binding proteins that have been shown to be sequestered include the heterogeneous nuclear ribonucleoprotein (hnRNP A2/B1), which results in alteration of dendritic transport upon sequestration via the CGG repeats, and Pur α, which plays a significant role in DNA replication, neuronal messenger RNA (mRNA) transport, and translation as well as Sam68, TDP43, and the DiGeorge syndrome critical region 8 protein, DGCR8 (11–15).

The second mechanism of FXTAS pathogenesis is via RAN translation of the CGG repeats into polypeptides, the predominant species being FMRpolyG (16, 17). First discovered in the CAG repeat expansion in human spinocerebellar ataxia type 8 and myotonic dystrophy type 1 (18), RAN translation has since been shown to play a potentially pathogenic role in amyotrophic lateral sclerosis (ALS)/frontotemporal dementia (FTD) as well as FXTAS (19). Recently, Sellier et al. have shown that FMRpolyG interacts with the nuclear lamina protein LAP2β and that the mechanism of pathogenesis may act through the resulting perturbation of the lamina architecture (16). Both *FMR1* mRNA and FMRpolyG peptide have been found in the human postmortem brain inclusions

Author affiliations: [a]Department of Human Genetics, School of Medicine, Emory University, Atlanta, GA 30322; [b]Department of Neurology, University of Michigan, Veteran's Affairs Medical Center, Ann Arbor, MI 48109; [c]Department of Biostatistics and Bioinformatics, Rollins School of Public Health, Emory University, Atlanta, GA 30322; [d]Department of Molecular and Human Genetics, Baylor College of Medicine, Houston, TX 77030; [e]Department of Neurology, School of Medicine, Emory University, Atlanta, GA 30322; [f]Department of Biochemistry, School of Medicine, Emory University, Atlanta, GA 30322; and [g]Department of Pediatrics, School of Medicine, Emory University, Atlanta, GA 30322

Author contributions: S.T.W. and P.J. designed research; H.E.K., J.L., A.L., Y.K., I.M., Y.C., L.S., P.K.T., and P.J. performed research; E.G.A., Y.G., M.E.Z., J.J., D.L.N., S.L.S., S.T.W., and P.J. contributed new reagents/analytic tools; H.E.K., J.L., A.L., Y.K., I.M., E.G.A., Y.C., R.J., Y.H., X.G., M.E.Z., Z.Q., T.S.W., D.L.N., M.P.E., D.J.C., P.K.T., S.L.S., S.T.W., and P.J. analyzed data; and H.E.K., S.T.W., and P.J. wrote the paper.

The authors declare no competing interest.

This article is a PNAS Direct Submission.

[1]Deceased June 6, 2021.

[2]To whom correspondence may be addressed. Email: peng.jin@emory.edu.

This article contains supporting information online at http://www.pnas.org/lookup/suppl/doi:10.1073/pnas.2118124119/-/DCSupplemental.

Published May 26, 2022.

that are characteristic of FXTAS pathology, suggesting that both mechanisms may contribute to the disease (17, 20).

Both mouse and fly models have been developed to study the molecular and genetic basis of FXTAS (16, 21–24). Our group has previously established a *Drosophila* model of FXTAS that expresses the premutation CGG repeat in the context of the human *FMR1* 5′UTR. Owing to its advantages of rapid reproduction and affordability as well as facile genetics, the FXTAS *Drosophila* model has been instrumental in showing that the premutation CGG repeats are sufficient to cause FXTAS pathology, as well as in the identification of hnRNP A2/B1 and Pur α as RNA binding proteins sequestered by the CGG premutation expansion (11, 15, 22). Expression of $r(CGG)_{90}$ under the eye-specific driver in *Drosophila*, *gmr-GAL4*, leads to a rough eye phenotype in the fly, characterized by cell death, loss of pigmentation, and ommatidial disruption (22).

Here, by combining whole-genome sequencing (WGS) with genetic screening using FXTAS *Drosophila* model, we have identified 18 genes as potential genetic modifiers of FXTAS. We show that knockdown of one of the identified genetic modifiers, *Proteasome subunit beta-type 5* (*PSMB5*), ameliorates CGG-associated neurotoxicity in *Drosophila* as well as in mammalian cells. Through the *PSMB5* expression quantitative trait locus (eQTL) variant $PSMB5^{rs11543947\text{-}A}$, we demonstrate a correlation between decreased *PSMB5* mRNA expression and delayed onset of FXTAS in human premutation carriers. Finally, we show that both mechanisms of FXTAS pathogenesis—RNA toxicity and RAN translation—may account for the suppression of CGG-associated toxicity in FXTAS upon lowering the expression of PSMB5. Our works suggest that using FXTAS *Drosophila* as a genetic screening tool can be powerful in the validation of candidate genes from WGS of FXTAS premutation carriers and controls, and consistent with previous studies, we have identified a role for the proteasome in FXTAS pathogenesis (25–27).

Results

Combination of WGS and *Drosophila* Screen Identifies 18 Genes as Genetic Modifiers of FXTAS. With the goal of identifying genetic modifiers of FXTAS, we recruited and collected whole blood samples from 108 *FMR1* premutation carriers for WGS (*SI Appendix*, Fig. S1 and Table S1). Following our pipeline outlined in *Materials and Methods*, we mapped, called, and annotated the variants using PEMapper, PECaller, and Bystro (28, 29). Given our limited statistical power, instead of taking a statistical approach for candidate gene selection, we employed a carefully curated criteria to select candidate genes (Fig. 1*A*), prioritizing variants based on combined annotation dependent depletion (CADD) score (31), phenotype severity of the premutation carriers harboring the variant, and any reported interaction of the gene with known ataxia genes as well as existence of *Drosophila* orthologs and RNA interference (RNAi) lines (*Materials and Methods*) (30).

As a result, we selected 97 genes to screen in the FXTAS *Drosophila* model by knocking down the candidate gene in the FXTAS fly eye using the UAS-GAL4 system, then screening for enhancement or suppression of the rough eye phenotype (Fig. 1*A* and *SI Appendix*, Table S2). The corresponding RNAi lines were obtained from the Transgenic RNAi Project (TRiP) (32). Out of the 97 candidate genes screened, 18 genes exhibited genetic modulation of CGG toxicity, such as *Prosbeta5* (human *PSMB5*), *pAbp* (human *PABPC1L*), *e(y)1* (human *TAF9*), and *CG14231* (human *OSGEPL1*) (Fig. 1 *B* and *C* and *SI Appendix*, Table S2).

The eQTL Variant $PSMB5^{rs11543947\text{-}A}$ Is Associated with Decreased Expression of *PSMB5* mRNA and Correlates with Delayed Onset of Ataxia and Tremor in Human Premutation Carriers. *Proteasome Subunit Beta-5* (*PSMB5*) was selected for the *Drosophila* screen based on a variant ($PSMB5^{rs11543947\text{-}A}$) that we found in our *FMR1* premutation carrier population (Fig. 2*A*). $PSMB5^{rs11543947\text{-}A}$ has a high CADD score of 34, indicating that it is predicted to be among the top 0.1% deleterious variants in the genome (Fig. 1*B*) (31). Intriguingly, as data from the Genotype-Tissue Expression Project (GTEx) indicate, $PSMB5^{rs11543947\text{-}A}$ is also an eQTL associated with decreased expression of *PSMB5* mRNA across a vast spectrum of tissues (*SI Appendix*, Fig. S2). In cortex tissue from the brain, we found that on average, individuals harboring the variant allele of $PSMB5^{rs11543947\text{-}A}$ demonstrate decreased expression of *PSMB5* (Fig. 2*B*). In addition, although $PSMB5^{rs11543947\text{-}A}$ was in Hardy–Weinberg equilibrium in our population, we were interested to find that in the comparison of premutation carriers exhibiting delayed onset of both tremor and ataxia with premutation carriers with early onset, $PSMB5^{rs11543947\text{-}A}$ was associated with delayed onset of both core phenotypes of FXTAS: tremor and ataxia (Fig. 2*C*). Early onset was defined as onset of both tremor and ataxia before age 65, and delayed onset was defined as the absence of both tremor and ataxia above age 69 (*SI Appendix*, Table S1). We further examined the expression of *PSMB5* in both FXTAS mouse model and FMR1 premutation-derived neural progenitor cells and did not observe the differential expression (*SI Appendix*, Fig. S3 A and *B*). Based on these findings, we hypothesized that premutation carriers with a lower baseline expression of *PSMB5* may be protected against the CGG-associated neurodegeneration associated with the premutation expansion in *FMR1*.

Knockdown of Proteasome Subunit beta-5 (*PSMB5*) Suppresses rCGG-Associated Neurodegeneration in *Drosophila*. We set out to test our hypothesis by taking advantage of the UAS-GAL4 system to modulate the expression of the fly ortholog of *PSMB5* (*Prosbeta5*) in the FXTAS *Drosophila* eye. We observed strong suppression of CGG-associated neurodegeneration upon *Prosbeta5* knockdown in the 90-CGG fly (Fig. 2*D* and *SI Appendix*, Table S2 and Fig. S3*C*). Conversely, overexpression of *Prosbeta5* resulted in inversion of the effect, such that the fly eyes exhibited enhancement of the rough eye phenotype (Fig. 2*D*). Knockdown of *Prosbeta5* in the wild-type (WT) fly eye resulted in enhancement of the rough eye phenotype, suggesting that knockdown of *Prosbeta5* is inherently toxic in the absence of CGG repeats. However, interestingly, in the background of CGG-associated neurotoxicity, knockdown of *Prosbeta5* ameliorates the toxicity (Fig. 2*D*). Taken together, the genetic evidence in the fly and human premutation carriers suggests that the PSMB5 expression could modulate CGG repeat-induced neuronal toxicity and the knockdown of *PSMB5* may ameliorate of CGG-induced neurodegeneration.

Amelioration of CGG Toxicity Is Specific to *PSMB5*. Intrigued by these findings, we wanted to verify whether the amelioration of CGG-associated neurotoxicity is specific to *PSMB5* knockdown or whether it also involves other subunits of the proteasome complex. The 26S proteasome consists of the 20S core particle and the 19S regulatory particle (RP) (33). Therefore, we tested all genes related to the 20S core particle subunits and the 19S regulatory particle that have fly orthologs as well as *Drosophila* TRiP lines available for screening (*SI Appendix*, Table S3). Thirty-five out of 41 human genes that encode

A

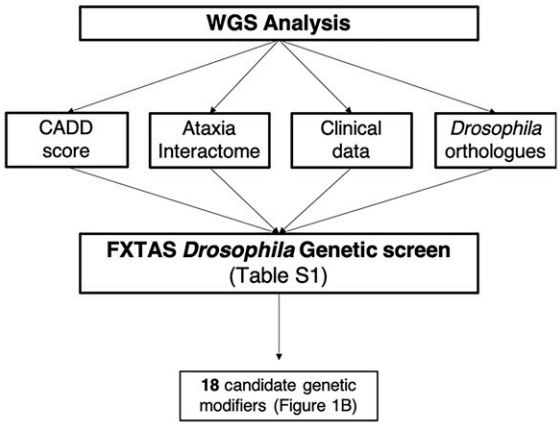

B

	Chr:pos Variant	Human Gene	*Drosophila* Gene	High CADD score
1	chr1:33036780	*AK2*	***Adk2***	33
2	chr6:35078619	*ANKS1A*	***CG4393***	34
3	chr5:69174962	*CCNB1*	***CycB***	33
4	chr4:110510288	*ENPEP*	***CG32473***	42
5	chr2:127292669	*ERCC3*	***hay***	37
6	chr2:120990472	*GLI2*	***ci***	29.6
7	chr3:97959130	*MINA*	***CG2982***	32
8	chr2:189753972	*OSGEPL1*	***CG14231***	34
9	chr20:44916864	*PABPC1L*	***pAbp***	34
10	chr9:128720227	*PKN3*	***pkn***	34
11	chr14:23034812	*PSMB5*	***prosbeta5***	34
12	chr15:55234786	*RAB27A*	***Rab27***	33
13	chr2:210002690	*RPE*	***CG30499***	34
14	chr15:45101228	*DUOX2*	***Duox***	Indel/frameshift
15	chr12:7795090	*NANOG*	***Bsh***	
16	chr14:23565950	*AP1G2*	***Ap-1gamma***	Ataxia Interactome Genes
17	chr11:66625654	*RBM14*	***lark***	
18	chr5:69365721	*TAF9*	***e(y)1***	

C

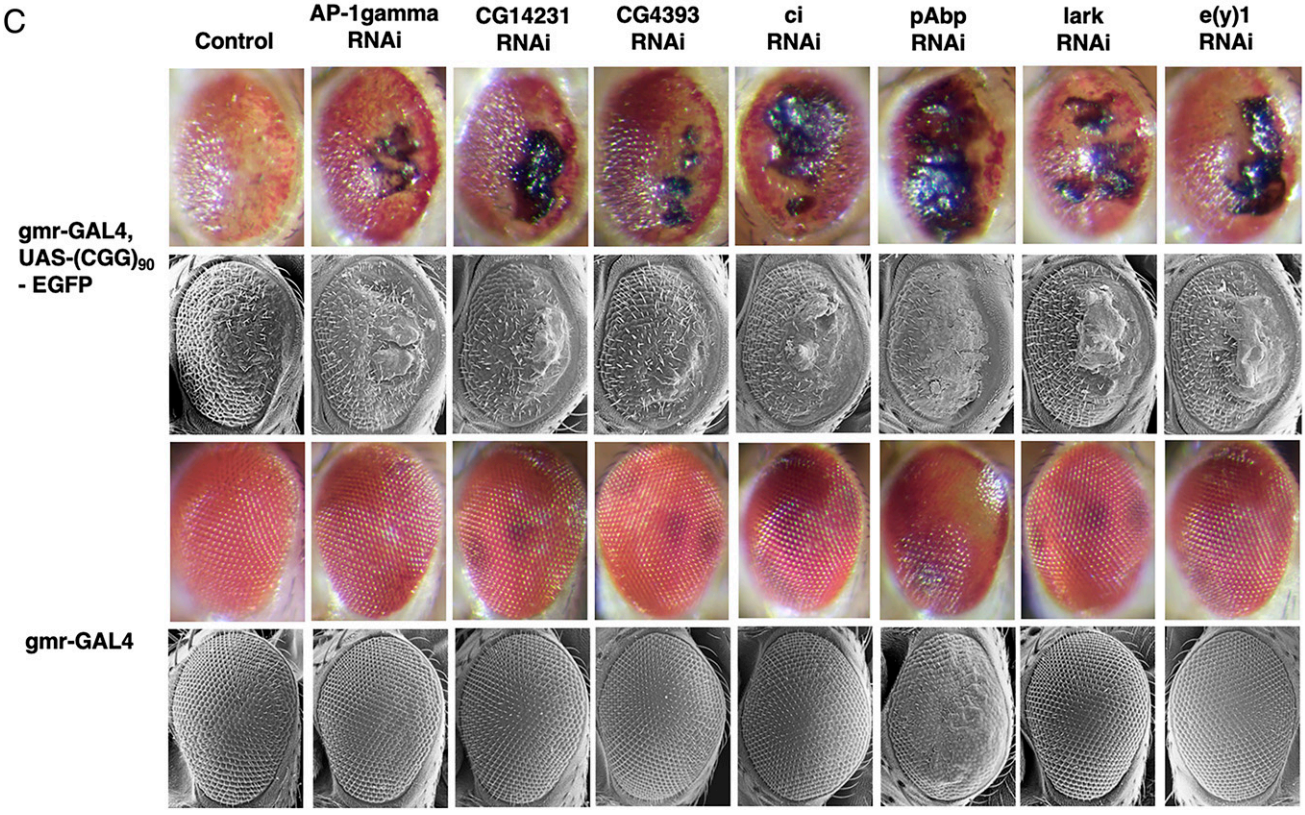

Fig. 1. Identification of genetic modifiers of FXTAS by combining WGS with *Drosophila* genetic screening. (*A*) Schematic depicting the analysis workflow from WGS analysis to *Drosophila* screen. Candidate genes were selected based on the variant CADD score, inclusion in the ataxia interactome (30), and clinical phenotype data of the variant carriers as well as the existence of *Drosophila* orthologs and availability of RNAi lines. A total of 97 genes were selected to test for genetic modulation in FXTAS *Drosophila*. Eighteen genes demonstrated significant modulation of CGG-associated neurodegeneration in the FXTAS fly eye. (*B*) List of 18 human genes and corresponding *Drosophila* orthologs that demonstrated genetic modulation of CGG-associated neurodegeneration in the FXTAS *Drosophila* screen. The table indicates the genomic location of the variant in the premutation carrier population. Thirteen genes had variants with high CADD scores, two had indel/frameshift variants, and three genes were part of the ataxia interactome (30). (*C*) *Drosophila* screen identifies 18 genetic modifiers of CGG-associated neurotoxicity. Representative light microscopy (first and third rows) and SEM images (second and fourth rows) from *Drosophila* of the indicated genotypes crossed to *GMR-GAL4, UAS-(CGG)$_{90}$ EGFP* (first and second rows) or *GMR-GAL4* flies (third and fourth rows) as control. After performing the crosses, progeny were collected and aged to 7 d. The screen was performed by scoring eye phenotype in crosses with $n > 10$ progeny, which was visualized using light microscopy and confirmed with SEM. Representative images are shown. RNAi knockdown of *Ap-1gamma*, *CG14231*, *CG4393*, *ci*, *pAbp*, *lark*, *and e(y)1* results in enhancement of CGG-associated neurodegeneration.

components of the 26S complex were screened based on the presence of fly orthologs and availability of TRiP lines. Four of the 35 genes demonstrated enhancement of CGG-associated neurodegeneration upon knockdown: *Prosalpha3* (*PSMA4*), *Prosalpha6T* (*PSMA1*), *Prosalpha7* (*PSMA3*), and *Rpn3* (*PSMD3*) (Fig. 3*A* and *SI Appendix*, Table S3). Over 88% of the genes tested showed no genetic modulation of the CGG-associated neurotoxicity upon knockdown, and significantly, none of the

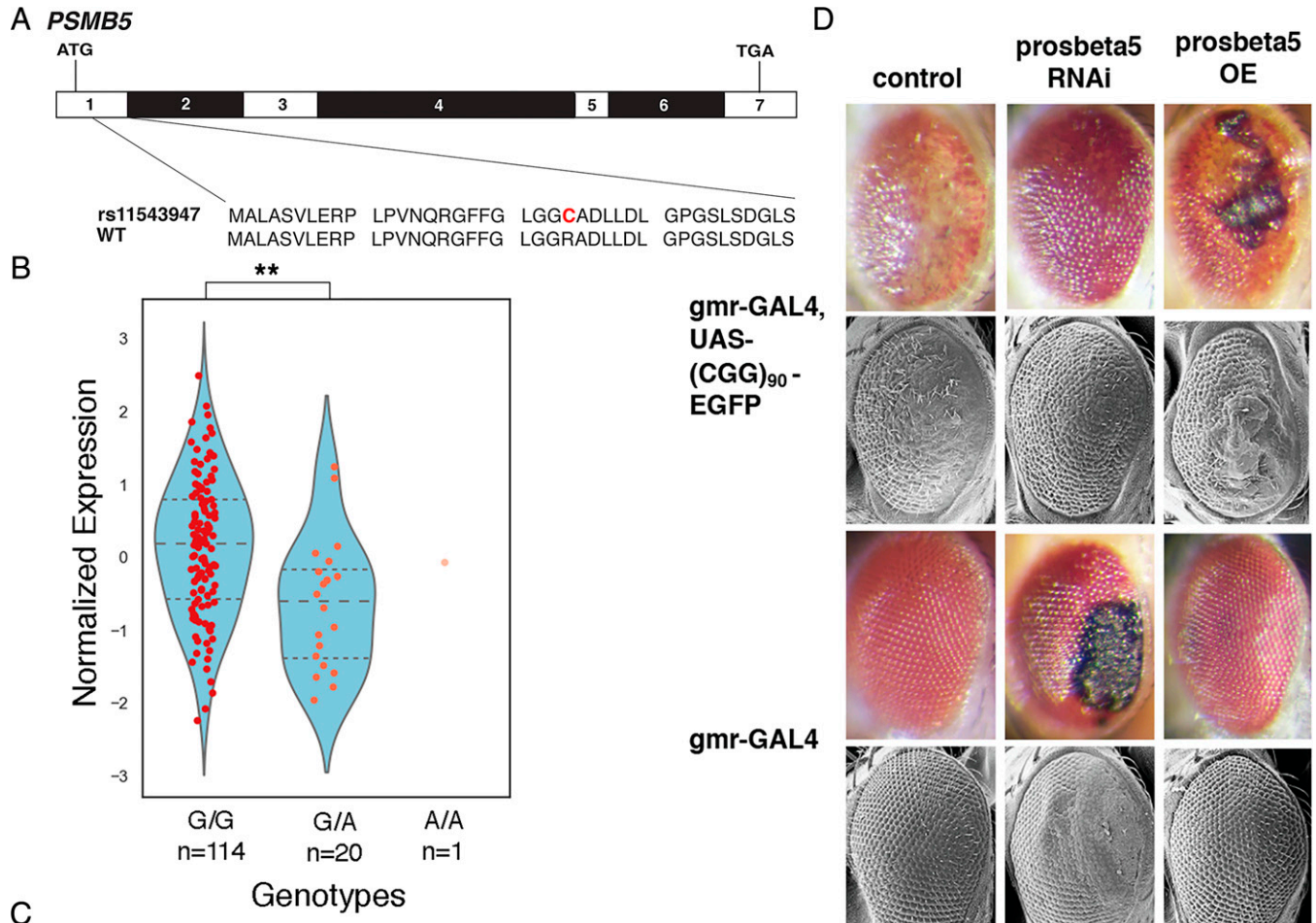

	Allele frequency in study population	Allele frequency in general population	Odds ratio	95% Confidence Interval
No Ataxia and Tremor	0.125	0.0646	2.07	0.62-6.94
Early Ataxia and Tremor	0.048	0.0646	0.74	0.23-2.35

Fig. 2. *PSMB5* modulates FXTAS. (*A*) Schematic displaying the location of $PSMB5^{rs11543947\text{-}A}$ in *PSMB5*. $PSMB5^{rs11543947\text{-}A}$ results in a G to A transition that leads to a missense replacement of Cys24 for Arg24. (*B*) $PSMB5^{rs11543947\text{-}A}$ is an eQTL resulting in decreased expression of *PSMB5* mRNA. Violin plot depicts the diminished expression level of *PSMB5* mRNA in brain (cortex) tissue of human samples from G/G genotype (*Left*) to G/A (*Middle*), two-group *t* test, $P = 0.00104$. Sample size for A/A genotype was insufficient ($n = 1$) to make comparisons to A/A. (*C*) $PSMB5^{rs11543947\text{-}A}$ is enriched in delayed onset premutation carriers who are asymptomatic compared to premutation carriers with early onset of ataxia and tremor. Table shows the frequency of $PSMB5^{rs11543947\text{-}A}$ variant allele in premutation carriers with no onset of FXTAS symptoms (ataxia and tremor) and early onset of both FXTAS symptoms, as well as the general population frequency (35). The odds ratio is elevated in the group with no ataxia and tremor phenotype, demonstrating that $PSMB5^{rs11543947\text{-}A}$ is enriched in premutation carriers without symptoms of FXTAS. (*D*) Knockdown of *prosbeta5* in *GMR-GAL4*, *UAS-(CGG)$_{90}$ EGFP* flies suppresses CGG-associated neurotoxicity, while *prosbeta5* knockdown in WT *GMR-GAL4* flies results in enhancement. Demonstrating epistasis, overexpression of *prosbeta5* in contrast results in enhancement of neurotoxicity in the *GMR-GAL4*, *UAS-(CGG)$_{90}$ EGFP* flies. The light microscopy (first and third rows) and SEM images (second and fourth rows) from *Drosophila* of the indicated genotypes crossed to *GMR-GAL4, UAS-(CGG)$_{90}$ EGFP* (first and second rows) and *GMR-GAL4* (third and fourth rows) flies as control.

screened genes showed suppression of CGG-associated toxicity upon knockdown. Our results clearly suggest that the alleviation of CGG toxicity is specific to *Prosbeta5*, and knockdown of other subunits of the *Drosophila* proteasome complex did not recapitulate the suppression of CGG toxicity seen in *Prosbeta5* knockdown.

***Psmb5* Knockdown and Inhibition Alleviate CGG-Associated Toxicity in Mammalian Neuronal Cells.** To further test this hypothesis in a mammalian model system, we transfected murine Neuro2A cells with the 5′UTR CGG 99x FMR1-EGFP plasmid expressing 99 CGG repeats in the context of the human 5′UTR *FMR1*, in frame with EGFP, as well as an empty vector control. Notably, upon small interfering RNA (siRNA) knockdown of *Psmb5*, we observed a significant amelioration of CGG-associated toxicity in N2A cells after 96 h ($n = 3$ independent replicates; Fig. 3*B* and *SI Appendix*, Fig. S3*D*). Consistent with the finding in the flies, knocking down *Psmb5* in Neuro2A cells transfected with empty vector control resulted in decreased cell viability (Fig. 3*B*).

We further validated whether this amelioration of CGG-associated toxicity is specific to the *PSMB5* using a US Food and Drug Administration (FDA)–approved selective inhibitor of *PSMB5*, ixazomib citrate (34). We administered 0.25 nM of ixazomib citrate to Neuro2A mammalian cells following transfection of the 5′UTR CGG 99x FMR1-EGFP plasmid expressing

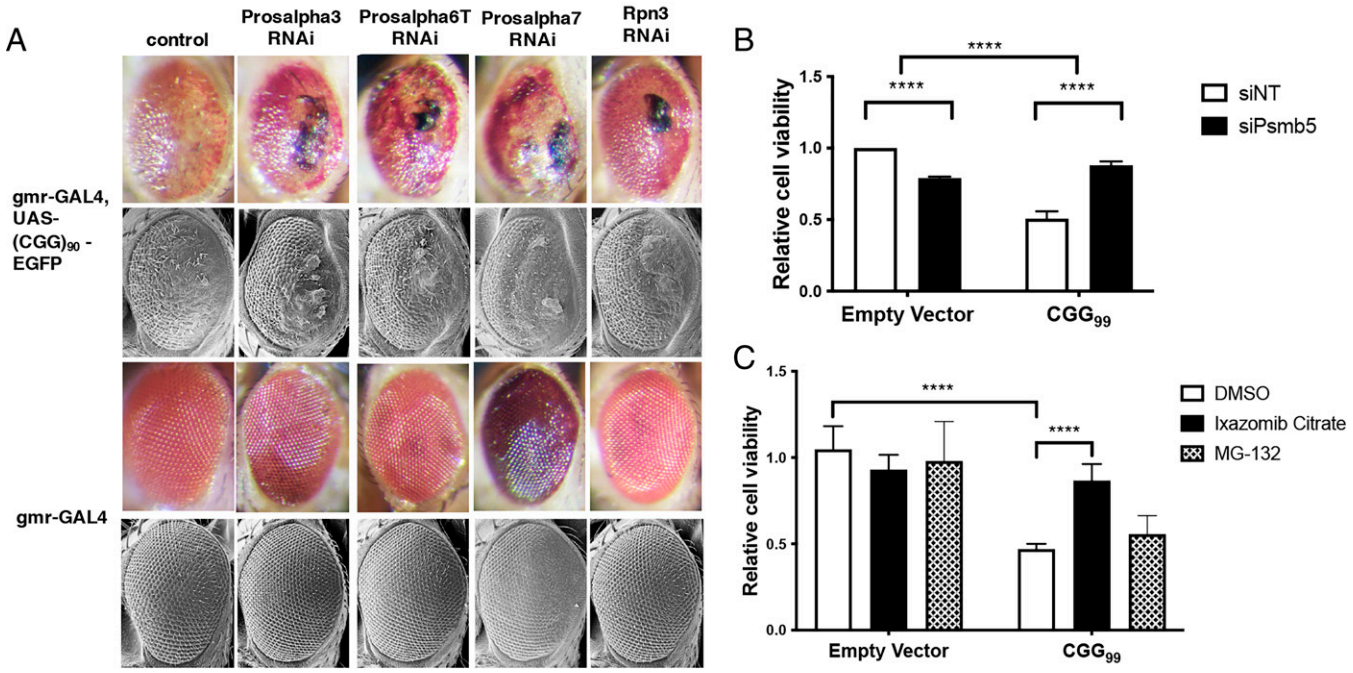

Fig. 3. Specific inhibition of *PSMB5* suppresses rCGG repeat-mediated neuronal toxicity associated with FXTAS. (*A*) Screen of *Drosophila* orthologs of proteasome subunits demonstrates enhancement of CGG-associated neurotoxicity with RNAi knockdown of four genes: *Prosalpha3* (*PSMA4*), *Prosalpha6T* (*PSMA1*), *Prosalpha7* (*PSMA3*), and *Rpn3* (*PSMD3*). RNAi lines of *Drosophila* proteasome subunits were crossed with *GMR-GAL4*, *UAS-(CGG)$_{90}$ EGFP* flies and resulted in significant enhancement of CGG-associated neurotoxicity for four genes (*SI Appendix*, Table S4). The light microscopy (first and third rows) and SEM images (second and fourth rows) from *Drosophila* of the indicated genotypes crossed to *GMR-GAL4*, *UAS-(CGG)$_{90}$ EGFP* (first and second rows) and *GMR-GAL4* flies as control (third and fourth rows). (*B*) siRNA knockdown of *PSMB5* results in suppression of CGG-associated neurotoxicity in Neuro2A cells. Data were pooled across three replicates (two-way ANOVA model, Sidak's multiple comparison test, ****$P < 0.0001$). (*C*) Pharmacologic inhibition of PSMB5 with 2.5 nM ixazomib citrate, but not 250 nM MG-132, results in suppression of CGG-associated neurotoxicity in Neuro2A cells. Data were pooled across three replicates (two-way ANOVA, Sidak's multiple comparisons test, ****$P < 0.0001$).

CGG repeats in the context of the human 5′UTR (*SI Appendix*, Fig. S4). In Neuro2A cells treated with dimethyl sulfoxide (DMSO) after expression of the rCGG repeats, only ∼50% of control cells survived after 84 h ($n = 3$ independent replicates) (Fig. 3*C*). However, upon administration of ixazomib citrate for 84 h, we observed a significant alleviation of CGG-associated toxicity with 85% of cells surviving (Fig. 3*C*). Intriguingly, the administration of MG-132, another 26S proteosome inhibitor that blocks the proteolytic activity of the 26S proteasome complex, did not result in the reduced CGG-associated toxicity, suggesting that *PSMB5* could act in a manner that is independent of the 26S proteosome (Fig. 3*C*).

Knockdown of *PSMB5* Significantly Diminishes RAN Translation in a Frame-Independent Manner. Given that our genetic findings of CGG toxicity alleviation upon *PSMB5* knockdown were recapitulated in the *Drosophila* as well as in Neuro2A cells through various methods, we sought a mechanistic explanation and asked whether knockdown of *PSMB5* alters RAN translation. RAN translation has been shown to play a potentially pathogenic role in FXTAS, with the predominant species being FMRPolyG (16, 17). To test this, we utilized a set of transfectable, plasmid-based nanoluciferase (NL) reporters (36) for canonical and RAN translation. The reporter for canonical translation, AUG-NL-3xF, comprises a short, unstructured 5′UTR; an AUG-initiated NL open reading frame; and a C-terminal 3xFLAG (3xF) tag to enable detection by Western blotting. The reporter for RAN translation of *FMR1* in the +1 frame comprises the 5′UTR of human *FMR1* bearing 100 CGG repeats, a GGG-initiated NL open reading frame (which abrogates initiation at this site) (36, 37), and the same 3xF tag. Translation of this *FMR1* reporter initiates within the *FMR1* 5′UTR (36).

When *PSMB5* was knocked down by siRNAs against *PSMB5*, we saw a decline in canonical translation but a significantly steeper decline in RAN translation (Fig. 4*A* and *SI Appendix*, Fig. S5). Furthermore, we observed that the decline in RAN translation is frame-independent; knockdown of *PSMB5* resulted in significant decline of RAN translation in both the +1 and +2 frames (Fig. 4*B*).

Knockdown of *PSMB5* May Ameliorate CGG-Associated Toxicity by Alleviating the Effects of DGCR8 Sequestration to the Expanded *FMR1* Premutation CGG Repeat. Besides RAN translation, we also determined whether the alleviating effects of *PSMB5* knockdown may be associated with the sequestration of RNA binding proteins to the expanded CGG repeat. Based on a database of high-throughput data such as cross-linking and immunoprecipitation sequencing(CLIP-seq), Ribosome sequencing (Ribo-seq), and RNA sequencing (RNA-seq) POST-trAnscriptional Regulation database 2 (POSTAR2), we found that *PSMB5* mRNA has been shown to be bound by DGCR8, an RNA binding protein already reported to be sequestered by the *FMR1* premutation repeats (14, 38).

We hypothesized that if DGCR8 normally binds *PSMB5* mRNA, then upon sequestration of DGCR8 to the expanded CGG repeats, we may be able to observe a significant decline of *PSMB5* mRNA bound to DGCR8 (Fig. 4*C*). To test this, we transfected HEK 293T cells with a plasmid expressing FLAG-tagged human DGCR8. Forty-eight hours later, we subsequently transfected the cells with either a plasmid expressing rCGG$_{99}$ in the context of the human *FMR1* 5′UTR or an empty vector control (Fig. 4*D*). After 24 h, we performed immunoprecipitation for DGCR8 using anti-FLAG antibody and found that upon expression of the *FMR1* premutation CGG repeats, the level of *PSMB5*

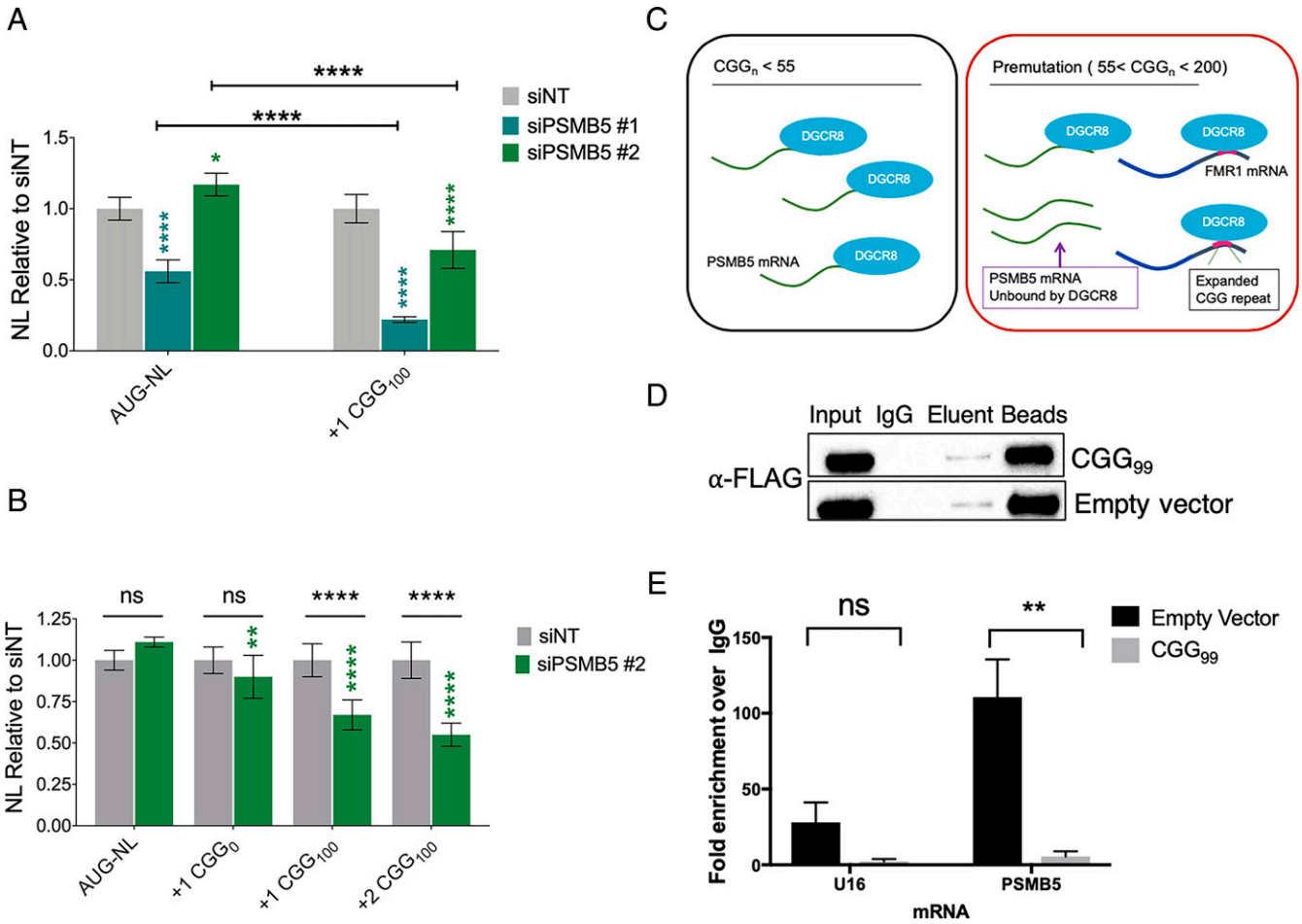

Fig. 4. Mechanisms of amelioration of CGG-associated toxicity by *PSMB5* knockdown. (*A* and *B*) PSMB5 knockdown significantly diminishes RAN translation of FMR1 5′UTR CGG repeats. Plasmid-transfected NL-based reporters for canonical and RAN translation were expressed in HEK293 cells, following transfection of siRNAs against PSMB5 or nontargeting siRNAs (siNT). Four replicates were performed with consistent results, and the graph represents the pooled data gathered across two replicates (two-way ANOVA with Tukey's multiple comparisons test; $n = 6$ per condition; $^{*}P \leq 0.0332$, $^{**}P \leq 0.0021$, $^{****}P \leq 0.0001$). Knockdown of *PSMB5* results in significant suppression of RAN translation compared to canonical translation and is not frame-dependent. (*C*) Schematic illustrates a proposed model depicting a potential mechanism of CGG-associated toxicity in FXTAS. DGCR8 normally binds PSMB5 mRNA (*Left*). In the presence of the expanded premutation *FMR1* CGG repeat (*Right*), DGCR8 is sequestered to the expanded CGG repeat, potentially leading to an increase of PSMB5 mRNA unbound by DGCR8. (*D* and *E*) Immunoprecipitation of FLAG-DGCR8 shows less PSMB5 mRNA binds to DGCR8 in the presence of CGG repeats. (*D*) FLAG-DGCR8 was overexpressed in HEK293T cells for 24 h, then cells were subsequently transfected again with either 5′UTR CGG 99x *FMR1*-EGFP plasmid or pcDNA 3.1. Western blot shows upon immunoprecipitation with anti-FLAG antibody, equal amounts of FLAG-DGCR8 were pulled down and eluted. (*E*) PSMB5 mRNA bound to FLAG-DGCR8 diminishes significantly in the presence of the expanded CGG repeat. Following immunoprecipitation, the eluent was subject to RNA extraction. Using RT-qPCR, mRNA bound to FLAG-DGCR8 was quantified. Significantly less PSMB5 mRNA was bound to FLAG-DGCR8 in the presence of the CGG repeat. Differences in the levels of U16 snoRNA (also known to be bound by DGCR8) were not statistically significant. Data were pooled across three replicates (two-way ANOVA with Sidak's multiple comparisons test, $n = 3$ per condition, $^{**}P \leq 0.005$).

mRNA bound to DGCR8 dropped significantly (Fig. 4*E*). As a positive control, we also tested the levels of the small nucleolar RNA (snoRNA) U16, a well-validated target of DGCR8 (Fig. 4*E*). Overall, these findings lend support to the possibility that DGCR8 plays a role in *PSMB5* mRNA processing that is perturbed upon sequestration of DGCR8 to the CGG repeats (Fig. 4 *D* and *E*).

Discussion

FXTAS is a late-onset neurodegenerative disorder caused by the 55 to 200 expanded CGG repeats in the 5′UTR of *FMR1*. Fragile X premutation carriers have an estimated prevalence of 1:250 women and 1:800 men (7–9). It is not at all understood why only some premutation carriers develop FXTAS; ∼40% of males and 16% of females develop FXTAS in late adulthood (1, 2). The incomplete penetrance of FXTAS suggests the presence of genetic modifiers. Here we performed WGS on male premutation carriers ($CGG_{55–200}$) and demonstrate that using FXTAS *Drosophila* as a genetic screening tool can be powerful in the validation of candidate genes discovered through WGS. We report 18 candidate genes as genetic modifiers of FXTAS using this approach, which can serve as promising candidates for biomarker discovery and therapeutic development.

The pathogenesis of neurodegenerative diseases is commonly linked to defects in the degradation of misfolded proteins. Three mechanisms promote effective removal of misfolded proteins, namely, the ubiquitin (Ub)-proteasome system (UPS), chaperone mediated autophagy, and macroautophagy (39). In many neurodegenerative diseases such as Huntington's disease, Parkinson's disease (PD), Alzheimer's disease (AD), and ALS, the pathology stems from misfolded aggregates that are resistant to degradation via these mechanisms, and their accumulation particularly affects postmitotic neurons (40). Capitalizing on this pathologic mechanism, therapeutic strategies on many neurodegenerative diseases have been designed to augment the degradation of protein aggregates by further activating the mechanisms of protein clearance (41–43). In FXTAS, activation of proteolytic mechanisms has yet

to be implemented as a therapeutic approach. However, previous studies have indicated the potential of UPS as a therapeutic target for FXTAS (26). In *Drosophila*, impairment of β2 and β6 subunits of the proteasome were shown to enhance CGG-associated ommatidial degeneration (26), whereas overexpression of *Hsp70*, a molecular chaperone that assists in refolding, was shown to suppress the neurotoxicity even in the absence of misfolded proteins (22). In addition to the UPS, many have shown that activating autophagy via rapamycin may rescue neurodegenerative phenotypes (44, 45). However, contrary to other neurodegenerative disorders, previous reports clearly demonstrate that in FXTAS, activating autophagy via rapamycin actually enhances the CGG-associated neurodegeneration in *Drosophila* (26, 46). Instead, activating the mTOR pathway, rather than inhibiting mTOR via rapamycin, ameliorated CGG-associated neurotoxicity in *Drosophila*. These findings were the first indication that although FXTAS is a neurodegenerative disease with a protein accumulation problem, the pathogenic mechanism may differ significantly from the other neurodegenerative pathologies, which could be alleviated via rapamycin.

We report that while knockdown of most components of the 26S proteasome resulted in enhancement or no change in CGG-associated neurodegeneration, knockdown of *PSMB5*, one of the core catalytic subunits of the 26S proteasome complex, significantly ameliorates CGG-induced neurodegeneration in various models—as demonstrated in *Drosophila*, mammalian cells, as well as a correlation of delayed onset FXTAS phenotypes in human premutation carriers. Importantly, this study has investigated both potential mechanisms of FXTAS toxicity to explain this finding. We have shown in mammalian cells that RAN translation is significantly diminished by knockdown of *PSMB5*, although excessive knockdown of *PSMB5* will even affect global translation. We have also shown that at the mRNA level, the level of *PSMB5* mRNA bound to DGCR8 is significantly diminished in the presence of the premutation CGG repeats, suggesting that upon sequestration of DGCR8 to the CGG repeats, the role of DGCR8 in the regulation of *PSMB5* mRNA may be perturbed (14).

Our finding has significant value for the development of future therapeutics as well as potential biomarkers for disease prognosis. Although not a curative strategy, our data from *Drosophila* and mammalian cells suggest that modestly diminishing *PSMB5* expression may be a promising therapeutic approach to delay the onset of a debilitating neurodegenerative disorder. Several FDA-approved proteasome inhibitors are readily available, such as bortezomib (Velcade), carfilzomib (Kyprolis), and ixazomib citrate (Ninlaro), the first oral proteasome inhibitor approved by the FDA (47, 48). According to the evidence presented in this study, low-dose inhibition of PSMB5 at the protein level, via ixazomib citrate, may be a potential therapeutic strategy for the treatment of FXTAS.

We hypothesize based on our model that in the setting of the expanded CGG repeats in FXTAS, CGG-mediated sequestration of DGCR8 may diminish DGCR8-mediated regulation of *PSMB5* mRNA, resulting in pathology. Future experiments will be necessary to explore the mechanism behind the DGCR8 processing of *PSMB5* mRNA and CGG-associated toxicity. Our observations may also point toward a potential unique role of the PSMB5 subunit, especially in RAN translation. To the best of our knowledge, studies have yet to explore potential independent roles of the proteasome subunits, including PSMB5. Given our findings, it would be valuable to further investigate any potential noncanonical roles of PSMB5 and to explore its role in RAN translation.

It remains to be seen whether manipulating the RNA expression or protein level of PSMB5 may also ameliorate neurotoxicity in other neurodegenerative diseases, especially repeat-associated disorders, or whether this is a unique mechanism in FXTAS. Notably, we have recently begun to uncover additional disorders that are associated with CGG expansions. Recent studies have identified novel associations of CGG/GCC repeat expansions in *LOC642361/NUTM2B-AS1* and *LRP12* with oculopharyngeal myopathy with leukoencephalopathy and oculopharyngodistal myopathy, respectively (49). In addition, GGC repeat expansions have been associated with neuronal intranuclear inclusion disease (NIID) (50) as well as a larger family of NIID-related disorders (NIIDRD) that include AD and PD (51). Our identification of *PSMB5* as a key player in the modification of CGG-associated neurodegeneration may have implications for these NIID, NIIDRD, and ocular disorders caused by CGG/GCC repeat expansions.

Our finding that $PSMB5^{rs11543947\text{-}A}$ is enriched in premutation carriers with delayed onset of FXTAS was limited in statistical significance due to the small sample size. Attaining adequate statistical power to identify such variants that are not independently causative but may predispose or protect against a disease remains a challenge in the study of rare diseases. In light of these limitations, future studies are needed to further validate the potential of $PSMB5^{rs11543947\text{-}A}$ as a biomarker for disease prognosis in FXTAS. Nonetheless, combining our findings among premutation carriers with those from model systems provides strong evidence to continue with this line of investigation.

In conclusion, we have demonstrated that knockdown of *PSMB5* suppresses CGG-associated neurodegeneration in *Drosophila* as well as in a mammalian in vitro model. Inhibiting the β5 subunit at the protein level by the proteasome inhibitor ixazomib citrate also suppresses the CGG-generated toxicity in vitro. Further, we have shed light on a possible mechanism of the suppression of CGG-associated neurotoxicity, via significant suppression of RAN translation. Last, through WGS, we have identified $PSMB5^{rs11543947\text{-}A}$ as a variant that has high potential as a biomarker for delayed onset of disease. The association between $PSMB5^{rs11543947\text{-}A}$ and delayed onset of FXTAS aligns well with the molecular findings in various model systems due to its role as an eQTL that correlates with decreased expression of *PSMB5*. Taken together, our data suggest that *PSMB5* offers a promising therapeutic target for alleviating the CGG-associated neurodegeneration in FXTAS.

Materials and Methods

Study Population. The protocols and consent forms were approved by the Institutional Review Board at Emory University, and written informed consent was obtained from all subjects (IRB00074941). Subjects were identified from previous FX research projects at Emory, through recruitment efforts at scientific conferences, and through collaborations with other research groups. Subjects were screened for eligibility based on premutation carrier status, presence or absence of symptoms of tremor and/or ataxia, age, and gender. Only one family member per pedigree was enrolled in the study. After a subject was determined to be eligible, either a blood or saliva sample was collected. In addition, a brief medical history was collected from the subject or a family member, and pertinent medical records were collected. If medical records did not provide sufficient information for determining eligibility, a video examination was conducted by study personnel and reviewed by a neurologist. Early onset subjects were defined as male or female premutation carriers with symptoms of tremor or ataxia before age 65, as reviewed by a neurologist. Control individuals were defined as male premutation carriers that reached age 69 without significant tremor or ataxia symptoms, as reviewed by a neurologist.

Sample Preparation for WGS. DNA was extracted from biological samples using Qiagen Qiamp DNA Blood Mini Kit, Gentra Puregene extraction kit, or prepIT-L2P protocol from Oragene. Fragile site, folic acid type, rare, Fra(X)(Q27.3) A (FRAXA) CGG repeat numbers were determined by a fluorescent sequencer method (52). For male samples that did not amplify or females with only one allele, a second PCR protocol was used (53). The PCRs for FRAXA consisted of 1× PCR Buffer (Gibco/BRL), 10% DMSO, 370 μM deazaG, 500 μM d(ACT), 0.3 μM each primer, 15 ng T4 gene 32, and 1.05 U Roche Expand Long Taq. Primers for the FMR1 gene were C, 5′Cy5GCTCAGCTCCGTTTCGGTTTCACTTCCGGT3′, and F, 5′AGCCCCGCACTTCCACCAGCTCCTCCA3′ (54). Samples were stored and sent in batches for WGS at Hudson Alpha.

WGS. For HiSeq X Ten sequencing, DNA samples were normalized to 1,000 ng DNA in 50 μL water, sheared to ∼350 to 400 bp fragments with a Covaris LE-220 instrument, and end-repaired and A-tailed using New England Biolabs End-Repair and A-Tailing kits, under the manufacturer's recommended conditions. Following each step, the library was purified via Agencourt AMPure XP beads and eluted in water. Standard Illumina paired-end adaptors were ligated to the A-tailed DNA via New England Biolabs Rapid Ligation kit, purified using AMPure XP beads, and amplified with KAPA Biosystems HIFI PCR kit using six cycles of PCR. The primers were standard Illumina primers with a custom seven-base sample barcode in the i7 position. The final library was quality controlled using size verification via PerkinElmer LabChip GX and real-time PCR using the KAPA SYBR FAST qPCR Master Mix, primers, and standards according to the manufacturer's directions. Libraries were normalized to 2.5 nM stocks for use in clustering and sequencing.

Samples were processed on the Illumina ×10 with 150 bp reads. Raw data from HudsonAlpha were transferred to the Human Genetics Computational Cluster at Emory University and mapped to the Human Genome Build GRCH38 (hg38) with a 95% stringency. All samples were mapped using PEMapper and called using PECaller (28). Appropriate quality control metrics were used to ensure that only high-quality samples were kept in the dataset. These included read depth, mapping percentage, Ts/Tv ratio, silent/replacement ratio, theta, theta in exons, fraction of nonreference homozygote calls, and number of novel variants called. With the exception of samples of African ancestry, samples were excluded from the final dataset if they were more than three SDs from the mean for any metric. Samples were also excluded if they had >5% missing calls at sites. Variants were excluded if they were missing >10% of calls across all samples or for Hardy-Weinberg equilibrium (HWE) violations with $P < 0.00001$. The entire dataset was annotated using Bystro (bystro.io) (29). Genomic data were uploaded to the National Institute of Mental Health (NIMH) Data Archive (https://nda.nih.gov/edit_collection.html?id=2380).

***Drosophila* Screen.** Transgenic flies expressing r$(CGG)_{90}$ were previously described (22). The *GMR-GAL4* and *UAS*-TRiP lines were obtained from Bloomington Stock Center. All *Drosophila* lines were maintained, and crosses were performed in standard medium at 25 °C. After performing the crosses, progeny were collected and aged to 7 d. The screen was performed by scoring eye phenotype in progeny with $n > 10$, which was visualized using light microscopy and confirmed with scanning electron microscopy (SEM).

SEM. Following dehydration in increasing concentrations of ethanol (25, 50, 75, and 100%), whole flies were incubated for 1 h with hexamethyldisilazane (Electron Microscopy Sciences). After removing the hexamethyldisilazane, the flies were dried overnight in a fume hood and subsequently analyzed using Topcon DS-130F and DS-150F Field Emission Scanning Electron Microscope.

Cell Culture, Transfection, and Cell Viability Assays. For transfection of FLAG-DGCR8, HEK293T were plated in Dulbecco's Modified Eagle Medium. After 24 h, cells were transfected with pFLAG/HA-DGCR8 (Addgene no. 10921) using Lipofectamine 3000 (Invitrogen) according to manufacturer instructions. Forty-eight hours later, cells were transfected again with 5′UTR CGG 99x FMR1-EGFP plasmid (Addgene no. 63091) or empty vector control (pCDNA 3.1+).

For the cell viability assay, Neuro2A cells were plated in Eagle's Minimum Essential Medium (EMEM) (Corning; 10-009-CV) with decreased fetal bovine serum (FBS) (2.5%). For *Psmb5* siRNA knockdown, 24 h following plating of cells in a 96-well plate, cells were cotransfected with 3 pmol per well siRNA and 200 ng per well plasmid DNA using Lipofectamine 2000 (Invitrogen). siRNAs used were mouse *Psmb5* siRNA or control siGENOME Non-Targeting siRNA Control Pools (Dharmacon; L-043960-01-0005, D-001206-14-05). Plasmid DNA consisted of 5′UTR CGG 99x FMR1-EGFP plasmid (Addgene no. 63091) or empty vector control (pCDNA 3.1+). Ninety-six hours after transfection, cell viability was measured using Cell Titer Blue (Promega; no. 8081) according to the manufacturer's instructions. For testing the effect of ixazomib citrate (Ark Pharm; no. AK54343) and MG-132 (Selleckchem; no. S2619) on cell viability, 24 h after plating onto a 96-well plate, the cells were transfected first with 200 ng per well plasmid DNA using Lipofectamine 2000 (Invitrogen). Plasmid DNA consisted of 5′UTR CGG 99x FMR1-EGFP plasmid (Addgene no. 63091) or empty vector control (pCDNA 3.1+). Twelve hours later after transfection, the EMEM was replaced with EMEM containing ixazomib citrate (Ark Pharm; AK545343) at 2.5 nM, MG-132 (Selleckchem; no. S2619) at 250 nM, or DMSO control. Eighty-four hours after addition of drugs/DMSO, cell viability was measured using Cell Titer Blue (Promega; no. 8081) according to the manufacturer's instructions.

Luciferase Assays and Western Blotting. HEK293 (CRL-1573; American type culture collection [ATCC]) cells were cultured and passaged at 37 °C, 5% CO_2 in DMEM supplemented with 10% FBS without antibiotics. For luciferase assays, HEK293 cells were plated on 96-well plates at 2.0×10^4 cells per well in 100 μL media and reverse transfected with ON-TARGET siRNAs against human *PSMB5* (nos. 1 and 2: J-004522-05-0002, J-004522-06-0002) or nontargeting controls (D-001810-10; Dharmacon) at 15 nM using Lipofectamine RNAiMAX (ThermoFisher Scientific). In brief, siRNA and RNAiMAX were diluted in Opti-MEM, combined, incubated for 10 mins at room temperature, and then added to cells. For subsequent plasmid transfection, 48 h after plating, cells were transfected with 50 ng per well pcDNA3.1(+)/NL-3xF plasmid using Viafect (Promega). Luciferase assays were performed 24 h after plasmid transfection, as described by Kearse et al. (36) and Green et al. (37).

For Western blotting experiments, HEK293 cells were plated in 12-well plates at 2×10^5 cells per well in 1 mL media and reverse transfected, as described above, with siRNAs at 15 nM. Forty-eight hours after plating, cells were transfected with 800 ng per well pcDNA3.1(+)/NL-3xF using jetPRIME (Polyplus; 114-15) according to manufacturer protocol. Twenty-four hours after plasmid transfection, cells were lysed on-plate in ice-cold radioimmunoprecipitation (RIPA) buffer. The lysate was homogenized using a 28.5 G syringe (without centrifugation), mixed with 6× reducing Laemmli buffer, heated at 90 °C for 10 min, resolved by sodium dodecyl sulfate (SDS)-polyacrylamide gel electrophoresis (SDS-PAGE), and transferred to a polyvinylidene difluoride (PVDF) membrane before incubation in primary antibody (FLAG M2, F1804, mouse [sigma] (1:1,000) in 5% milk in tris buffered saline with tween (TBST); PSMB5, PSMB5 (D1H6B) Rabbit mAb [Cell Signaling] (1:1,000); Beta-Actin, A1978, Mouse [sigma] dilution (1:2,000) using the same conditions).

Immunoprecipitation. The immunoprecipitation (IP) protocol for FLAG-DGCR8 was based on a described protocol with modifications (55). HEK293T cells transfected with pFLAG/HA DGCR8 (Addgene no. 10921) were grown in 60-mm plates. Forty-eight hours after transfection, cells were washed with ice-cold PBS, then scraped and centrifuged at 1,000 rpm for 5 min at 4 °C. For each immunoprecipitation, 30 μL of protein G Dynabeads were used. The beads were first washed with 1 mL wash buffer (20 mM Hepes-KOH, pH 7.9, 100 mM KCl, 0.2 mM ethylenediaminetetraacetic acid [EDTA], 0.5 mM dithiothreitol [DTT], 0.2 mM phenylmethanesulfonyl fluoride [PMSF], 5% glycerol) twice, then beads were resuspended in 300 μL of wash buffer and incubated with 5 μL of mAb-FLAG antibody (1 mg/mL) (F1804; Sigma) or IgG1 control (1 mg/mL) (12-371; Sigma), rotating at room temperature for 45 min. The cell pellets were resuspended in 1 mL lysis buffer (wash buffer supplemented with RNase OUT; ThermoFisher; 10777019) and sonicated on ice using Misonix Sonicator 3000 Ultrasonic Cell Disruptor with Temperature Control (Misonix) (three times, 27 s on, 27 s off). Extracts were spun down at 7,000 rpm for 5 min at 4 °C. The supernatant was transferred to a new tube and spun down again at 14,000 rpm, 10 min, 4 °C. Protein concentrations for cell lysates were quantified using a bicinchoninic acid assay (BCA) assay. Before adding antibody-conjugated beads to extracts, the beads were washed with 1 mL of wash buffer three times, rotating to remove any unbound antibody. Equal amount of lysates based on protein concentrations were added to antibody-conjugated beads. Immediately after adding the lysates to beads, the mixture was flicked using a finger to mix, then incubated for 2 h at 4 °C, tumbling end over end. Beads were washed 3× with lysis buffer. After the final wash, 20 μL of FLAG peptide (10 ng/μL) (F3290; Sigma) was added

(final concentration 0.5 mg/mL) for 2 h at 4 °C, rotating, to elute the protein from the beads.

For RNA extraction, 200 μL 1× RQ1-RNase-free DNase buffer was added to each tube, and the samples were treated with RQ1-RNase-free DNase (Promega; 6106) according to the manufacturer's instructions. SDS was added to yield a final concentration of 1%, then the samples were treated with proteinase K for 30 min at 55 °C, flicking the tube occasionally using a finger. Total RNA was extracted using Phenol:Chloroform:Isoamyl Alcohol 25:24:1 (P3803; Sigma).

For Western blotting, samples were denatured in 2× Laemmli Sample Buffer (Bio-Rad) at 95 °C, separated by SDS-PAGE on Mini-PROTEAN TGX Precast Mini Gels (Bio-Rad), transferred onto 0.2 μm PVDF membrane by Trans-Blot Turbo Blotting System and Mini Transfer Pack (Bio-Rad), and probed with primary antibodies against FLAG (1:4,000, mouse pAb, F1804; Sigma) at 4 °C overnight. Primary antibodies were labeled by horseradish peroxidase (HRP)-linked secondary anti-mouse antibody (1:4,000; Cell Signaling Technology). The enhanced chemiluminescent signals were detected using HyGLO Quick Spray Chemiluminescent HRP Antibody Detection Reagent (Thomas Scientific) and were visualized by the ChemiDoc Touch Imaging System (Bio-Rad).

For real-time PCR, cDNA was synthesized with SuperScript III reverse transcriptase (Invitrogen) using random hexamer primers, and real-time PCR was performed with primers in *SI Appendix*, Table S4.

Data Availability. Genomic data have been deposited in NIMH Data Archive (https://nda.nih.gov/edit_collection.html?id=2380). All other study data are included in the article and/or *SI Appendix*.

ACKNOWLEDGMENTS. First and foremost, we thank the families who participated in this project. Without their contribution and encouragement, this work could not have been done. We also thank the Fragile X Research Participant Registry of the Carolina Institute for Developmental Disabilities (grant P50HD103573) at the University of North Carolina at Chapel Hill who helped with recruitment. Last, we thank the Eunice Kennedy Shriver National Institute of Child Health and Human Development (NICHD) and the National Institute of Neurological Disorders and Stroke (NINDS) for supporting our National Fragile X Center (grants U54NS091859 and P50HD104463) in which this work was conducted. This study was supported in part by the Emory Integrated Genomics Core, which is subsidized by the Emory University School of Medicine and is one of the Emory Integrated Core Facilities. This study also utilized a Research Electronic Data Capture (REDCap) database supported by Emory's Library and Information Technology Services (grant UL1TR000424). We thank K. Charen, D. Hamilton, A. Amin, and W. He for DNA sample collection, preparation, and genotyping. We also thank M. A. Leehey, Y. Liu, M. Mila, L. Rodriguez-Revenga, E. Berry-Kravis, D. Hall, and R. J. Hagerman for their contributions. We thank Jorge Juncos for his review of phenotype data. Finally, we thank Y. Kang, F. Zhang, Y. Li, H. Kim, and all members of the P.J. laboratory for valuable discussion and scientific input. The GTEx Project was supported by the Common Fund of the Office of the Director of the NIH and by National Cancer Institute (NCI), National Human Genome Research Institute (NHGRI), National Heart, Lung and Blood Institute (NHLBI), National Institute on Drug Abuse (NIDA), NIMH, and NINDS. The data used for the analyses described in this manuscript were obtained from the GTEx Portal on 19 March 2019.

1. P. J. Hagerman, R. J. Hagerman, Fragile X-associated tremor/ataxia syndrome. *Ann. N. Y. Acad. Sci.* **1338**, 58–70 (2015).
2. S. Jacquemont *et al.*, Penetrance of the fragile X-associated tremor/ataxia syndrome in a premutation carrier population. *JAMA* **291**, 460–469 (2004).
3. D. Colak *et al.*, Promoter-bound trinucleotide repeat mRNA drives epigenetic silencing in fragile X syndrome. *Science* **343**, 1002–1005 (2014).
4. R. J. Hagerman, P. J. Hagerman, The fragile X premutation: Into the phenotypic fold. *Curr. Opin. Genet. Dev.* **12**, 278–283 (2002).
5. E. J. Kremer *et al.*, Mapping of DNA instability at the fragile X to a trinucleotide repeat sequence p(CCG)n. *Science* **252**, 1711–1714 (1991).
6. A. J. Verkerk *et al.*, Identification of a gene (FMR-1) containing a CGG repeat coincident with a breakpoint cluster region exhibiting length variation in fragile X syndrome. *Cell* **65**, 905–914 (1991).
7. C. Dombrowski *et al.*, Premutation and intermediate-size FMR1 alleles in 10572 males from the general population: Loss of an AGG interruption is a late event in the generation of fragile X syndrome alleles. *Hum. Mol. Genet.* **11**, 371–378 (2002).
8. J. Hunter *et al.*, Epidemiology of fragile X syndrome: A systematic review and meta-analysis. *Am. J. Med. Genet. A.* **164A**, 1648–1658 (2014).
9. F. Rousseau, P. Rouillard, M. L. Morel, E. W. Khandjian, K. Morgan, Prevalence of carriers of premutation-size alleles of the FMRI gene–and implications for the population genetics of the fragile X syndrome. *Am. J. Hum. Genet.* **57**, 1006–1018 (1995).
10. H. E. Kong, J. Zhao, S. Xu, P. Jin, Y. Jin, Fragile X-associated tremor/ataxia syndrome: From molecular pathogenesis to development of therapeutics. *Front. Cell. Neurosci.* **11**, 128 (2017).
11. P. Jin *et al.*, Pur alpha binds to rCGG repeats and modulates repeat-mediated neurodegeneration in a Drosophila model of fragile X tremor/ataxia syndrome. *Neuron* **55**, 556–564 (2007).
12. I. A. Muslimov, M. V. Patel, A. Rose, H. Tiedge, Spatial code recognition in neuronal RNA targeting: Role of RNA-hnRNP A2 interactions. *J. Cell Biol.* **194**, 441–457 (2011).
13. C. Sellier *et al.*, Sam68 sequestration and partial loss of function are associated with splicing alterations in FXTAS patients. *EMBO J.* **29**, 1248–1261 (2010).
14. C. Sellier *et al.*, Sequestration of DROSHA and DGCR8 by expanded CGG RNA repeats alters microRNA processing in fragile X-associated tremor/ataxia syndrome. *Cell Rep.* **3**, 869–880 (2013).
15. O. A. Sofola *et al.*, RNA-binding proteins hnRNP A2/B1 and CUGBP1 suppress fragile X CGG premutation repeat-induced neurodegeneration in a Drosophila model of FXTAS. *Neuron* **55**, 565–571 (2007).
16. C. Sellier *et al.*, Translation of expanded CGG repeats into FMRpolyG is pathogenic and may contribute to fragile X tremor ataxia syndrome. *Neuron* **93**, 331–347 (2017).
17. P. K. Todd *et al.*, CGG repeat-associated translation mediates neurodegeneration in fragile X tremor ataxia syndrome. *Neuron* **78**, 440–455 (2013).
18. T. Zu *et al.*, Non-ATG-initiated translation directed by microsatellite expansions. *Proc. Natl. Acad. Sci. U.S.A.* **108**, 260–265 (2011).
19. J. D. Cleary, L. P. Ranum, Repeat associated non-ATG (RAN) translation: New starts in microsatellite expansion disorders. *Curr. Opin. Genet. Dev.* **26**, 6–15 (2014).
20. F. Tassone *et al.*, Intranuclear inclusions in neural cells with premutation alleles in fragile X associated tremor/ataxia syndrome. *J. Med. Genet.* **41**, e43 (2004).
21. R. F. Berman *et al.*, Mouse models of the fragile X premutation and fragile X-associated tremor/ataxia syndrome. *J. Neurodev. Disord.* **6**, 25 (2014).
22. P. Jin *et al.*, RNA-mediated neurodegeneration caused by the fragile X premutation rCGG repeats in Drosophila. *Neuron* **39**, 739–747 (2003).
23. V. Hashem *et al.*, Ectopic expression of CGG containing mRNA is neurotoxic in mammals. *Hum. Mol. Genet.* **18**, 2443–2451 (2009).
24. A. Entezam *et al.*, Regional FMRP deficits and large repeat expansions into the full mutation range in a new Fragile X premutation mouse model. *Gene* **395**, 125–134 (2007).
25. S. Bergink *et al.*, The DNA repair-ubiquitin-associated HR23 proteins are constituents of neuronal inclusions in specific neurodegenerative disorders without hampering DNA repair. *Neurobiol. Dis.* **23**, 708–716 (2006).
26. S. Y. Oh *et al.*, RAN translation at CGG repeats induces ubiquitin proteasome system impairment in models of fragile X-associated tremor ataxia syndrome. *Hum. Mol. Genet.* **24**, 4317–4326 (2015).
27. M. Drozd *et al.*, Reduction of Fmr1 mRNA levels rescues pathological features in cortical neurons in a model of FXTAS. *Mol. Ther. Nucleic Acids* **18**, 546–553 (2019).
28. H. R. Johnston *et al.*; International Consortium on Brain and Behavior in 22q11.2 Deletion Syndrome, PEMapper and PECaller provide a simplified approach to whole-genome sequencing. *Proc. Natl. Acad. Sci. U.S.A.* **114**, E1923–E1932 (2017).
29. A. V. Kotlar, C. E. Trevino, M. E. Zwick, D. J. Cutler, T. S. Wingo, Bystro: Rapid online variant annotation and natural-language filtering at whole-genome scale. *Genome Biol.* **19**, 14 (2018).
30. J. Lim *et al.*, A protein-protein interaction network for human inherited ataxias and disorders of Purkinje cell degeneration. *Cell* **125**, 801–814 (2006).
31. M. Kircher *et al.*, A general framework for estimating the relative pathogenicity of human genetic variants. *Nat. Genet.* **46**, 310–315 (2014).
32. L. A. Perkins *et al.*, The transgenic RNAi project at Harvard medical school: Resources and validation. *Genetics* **201**, 843–852 (2015).
33. I. Livneh, V. Cohen-Kaplan, C. Cohen-Rosenzweig, N. Avni, A. Ciechanover, The life cycle of the 26S proteasome: from birth, through regulation and function, and onto its death. *Cell Res.* **26**, 869–885 (2016).
34. L. A. Raedler, Ninlaro (Ixazomib): First oral proteasome inhibitor approved for the treatment of patients with relapsed or refractory multiple myeloma. *Am Health Drug Benefits* **9**, 102–105 (2016).
35. M. Lek *et al.*; Exome Aggregation Consortium, Analysis of protein-coding genetic variation in 60,706 humans. *Nature* **536**, 285–291 (2016).
36. M. G. Kearse *et al.*, CGG repeat-associated non-AUG translation utilizes a cap-dependent scanning mechanism of initiation to produce toxic proteins. *Mol. Cell* **62**, 314–322 (2016).
37. K. M. Green *et al.*, RAN translation at C9orf72-associated repeat expansions is selectively enhanced by the integrated stress response. *Nat. Commun.* **8**, 2005 (2017).
38. Y. Zhu *et al.*, POSTAR2: Deciphering the post-transcriptional regulatory logics. *Nucleic Acids Res.* **47** (D1), D203–D211 (2019).
39. A. Ciechanover, Intracellular protein degradation: From a vague idea through the lysosome and the ubiquitin-proteasome system and onto human diseases and drug targeting. *Bioorg. Med. Chem.* **21**, 3400–3410 (2013).
40. A. Ciechanover, Y. T. Kwon, Degradation of misfolded proteins in neurodegenerative diseases: Therapeutic targets and strategies. *Exp. Mol. Med.* **47**, e147 (2015).
41. A. Caccamo, S. Majumder, A. Richardson, R. Strong, S. Oddo, Molecular interplay between mammalian target of rapamycin (mTOR), amyloid-beta, and Tau: Effects on cognitive impairments. *J. Biol. Chem.* **285**, 13107–13120 (2010).
42. S. Sarkar *et al.*, A rational mechanism for combination treatment of Huntington's disease using lithium and rapamycin. *Hum. Mol. Genet.* **17**, 170–178 (2008).
43. P. Spilman *et al.*, Inhibition of mTOR by rapamycin abolishes cognitive deficits and reduces amyloid-beta levels in a mouse model of Alzheimer's disease. *PLoS One* **5**, e9979 (2010).
44. Z. Berger *et al.*, Rapamycin alleviates toxicity of different aggregate-prone proteins. *Hum. Mol. Genet.* **15**, 433–442 (2006).
45. U. B. Pandey *et al.*, HDAC6 rescues neurodegeneration and provides an essential link between autophagy and the UPS. *Nature* **447**, 859–863 (2007).
46. Y. Lin, C. Tang, H. He, R. Duan, Activation of mTOR ameliorates fragile X premutation rCGG repeat-mediated neurodegeneration. *PLoS One* **8**, e62572 (2013).
47. P. de la Puente, A. K. Azab, Contemporary drug therapies for multiple myeloma. *Drugs Today (Barc)* **49**, 563–573 (2013).
48. B. Muz *et al.*, Spotlight on ixazomib: Potential in the treatment of multiple myeloma. *Drug Des. Devel. Ther.* **10**, 217–226 (2016).

49. H. Ishiura *et al.*, Noncoding CGG repeat expansions in neuronal intranuclear inclusion disease, oculopharyngodistal myopathy and an overlapping disease. *Nat. Genet.* **51**, 1222–1232 (2019).
50. J. Sone *et al.*, Long-read sequencing identifies GGC repeat expansions in NOTCH2NLC associated with neuronal intranuclear inclusion disease. *Nat. Genet.* **51**, 1215–1221 (2019).
51. Y. Tian *et al.*, Expansion of human-specific GGC repeat in neuronal intranuclear inclusion disease-related disorders. *Am. J. Hum. Genet.* **105**, 166–176 (2019).
52. K. L. Meadows *et al.*, Survey of the fragile X syndrome and the fragile X E syndrome in a special education needs population. *Am. J. Med. Genet.* **64**, 428–433 (1996).
53. W. T. Brown *et al.*, Rapid fragile X carrier screening and prenatal diagnosis using a nonradioactive PCR test. *JAMA* **270**, 1569–1575 (1993).
54. Y. H. Fu *et al.*, Variation of the CGG repeat at the fragile X site results in genetic instability: Resolution of the Sherman paradox. *Cell* **67**, 1047–1058 (1991).
55. S. Macias *et al.*, DGCR8 HITS-CLIP reveals novel functions for the Microprocessor. *Nat. Struct. Mol. Biol.* **19**, 760–766 (2012).